Smart Structures and Systems, *Vol. 20, No. 3 (2017) 273-283*
DOI: https://doi.org/10.12989/sss.2017.20.3.273

Feedback control strategies for active control of noise inside a 3-D vibro-acoustic cavity

Ashok K. Bagha* and Subodh V. Modak

Department of Mechanical Engineering, Indian Institute of Technology Delhi, Hauz Khas, New Delhi 110016, India

(Received March 25, 2016, Revised July 25, 2017, Accepted July 27, 2017)

Abstract. This paper presents and compares three feedback control strategies for active control of noise inside a 3-D vibro-acoustic cavity. These are a) control strategy based on direct output feedback (DOFB) b) control strategy based on linear quadratic regulator (LQR) to reduce structural vibrations and c) LQR control strategy with a weighting scheme based on structural-acoustic coupling coefficients. The first two strategies are indirect control strategies in which noise reduction is achieved through active vibration control (AVC), termed as AVC-DOFB and AVC-LQR respectively. The third direct strategy is based on active structural-acoustic control (ASAC). This strategy is an LQR based optimal control strategy in which the coupling between the various structural and the acoustic modes is used to design the controller. The strategy is termed as ASAC-LQR. A numerical model of a 3-D rectangular box cavity with a flexible plate (glued with piezoelectric patches) and with other five surfaces treated rigid is developed using finite element (FE) method. A single pair of collocated piezoelectric patches is used for sensing the vibrations and applying control forces on the structure. A comparison of frequency response function (FRF) of structural nodal acceleration, acoustic nodal pressure, and piezoelectric actuation voltage is carried out. It is found that the AVC-DOFB control strategy gives equal importance to all the modes. The AVC-LQR control strategy tries to consume the control effort to damp all the structural modes. It is seen that the ASAC-LQR control strategy utilizes the control effort more intelligently by adding higher damping to those structural modes that matter more for reducing the interior noise.

Keywords: direct output feedback controller; active vibration control; active structural-acoustic control; structural-acoustic coupling coefficients; linear quadratic regulator

1. Introduction

Recently, distributed signal processing has received a An important problem in systems such as automobile passenger compartments, aerospace interiors, helicopters, marine vehicles, launch vehicles and other enclosed spaces and cavities is the control of low frequency interior noise. In many of these systems the elastic structure surrounding the cavity vibrates under the action of mechanical and/or acoustic disturbances. These vibrations couple with the enclosed medium leading to generation of interior noise.

Active noise control technology has been gaining development in recent years and can be divided into three categories. The first one involves active noise cancellation (ANC), which uses interior acoustic sources such as loudspeakers to cancel the noise based on the error signal from acoustic sensors like microphones. The second method employs, active vibration control (AVC), vibration sources such as shakers or surface mounted piezoelectric actuators and acoustic sensor for error signal in the radiated acoustic field. The third method, which is known as active structural-acoustic control (ASAC), employs both structural actuators and structural error sensors. The objective of ASAC strategy is to modify or reconstruct the vibration of the flexible panels and reduce sound radiation or transmission into the cavity (Fuller and Flotow 1995, Li and Cheng 2010, Fahy and Gardonio 1987, Morand and Ohayon 2014).

Feedforward and feedback control are the two main control strategies that have been used for interior noise control. The feedforward technique has been used mainly to control interior noise due to harmonic and periodic disturbances (Fuller and Flotow 1995). Such disturbances arise from the operation of an IC engine in case of automotive vehicles and from a jet engine in case of aerospace vehicles. However, feedforward control requires measurement of a reference signal corresponding to the disturbance, which may not be always possible. The feedforward control also requires error sensors to be mounted at the points where the control is desired. It is also difficult to achieve global control using this technique. The random and broadband disturbances may also act on cavities like disturbances due to rough road, disturbances due to aerodynamic effects/turbulent boundary layer, acoustic load disturbance on a satellite during launching and broadband disturbances in a helicopter. These disturbances cannot be dealt effectively using feedforward techniques.

Feedback control is expected to be an effective strategy in cases where disturbances are random or broadband as well as in cases where it is difficult to measure reference signals corresponding to the disturbances. In view of this, in

*Corresponding author, Ph.D.
E-mail: ashokgem10.nit@gmail.com
[a]Ph.D.
E-mail: svmodak@mech.iitd.ac.in

ISSN: 1738-1584 (Print), 1738-1991 (Online)

this paper the control of interior noise in vibro-acoustic cavities is carried out using feedback control strategies. Feedback control strategies are used as: active damping and model based feedback. The objective of active damping is to reduce the effect of the resonant peaks on the response of the structure and, as a result, the steady state response to wide disturbances. Active damping can generally be achieved with direct output feedback (DOFB) (Fahy and Gardonio 1987). Optimal feedback control strategies involve applying a control input that minimizes a certain cost function taken as a combination of quantity to be controlled and the control effort. Such an optimal control strategy is referred as linear quadratic regulator (LQR) control. For noise control, the cost function provides a method of weighting heavily the modes of the structure that are known to be efficient acoustic radiators and similarly allows diminished weighting of the inefficiently radiating modes. For the structural-acoustic cavity systems, coupling between the structural modes and the cavity acoustic modes play a crucial role in the sound produced. Not all the structural modes couple strongly with an acoustic mode. Different structural and acoustic modes have different degrees of coupling. If a coupled finite element model of the structural-acoustic system is available then the coupling matrix can be computed in the modal domain to study the degree of coupling between various structural and acoustic modes. Structural vibration control instead of ASAC has been attempted by Song *et al.* (2003) to reduce the interior noise in a 3-D vehicle cabin model. Through contribution analysis, plate modes to be controlled are selected. The structural and acoustic modes can be classified into different clusters (Tanaka and Kobayashi 2006). The minimization of potential energy can be achieved through minimization of contribution from each cluster. Ray *et al.* (2009) calculated the structural-acoustic coupling coefficients to predict the structural mode that is more contributing towards the acoustic behavior inside the vibro-acoustic cavity.

In this paper, comparison of three feedback control strategies has been carried out. The three feedback control strategies are AVC-DOFB, AVC-LQR and ASAC-LQR. The first of these two strategies are indirect noise control strategies in which noise reduction is attempted through active vibration control (AVC). The objective is to reduce the vibrations with the hope of reducing the noise radiated into the cavity. The third strategy is active structural-acoustic control strategy. In which an LQR controller is designed by exploiting the knowledge of the structural-acoustic coupling of various structural and acoustic modes. Numerical study is carried out on a 3-D rectangular box cavity with a flexible plate (glued with a single pair of collocated piezoelectric patches) that is coupled to the acoustic domain.

2. Numerical model of the piezo-structural-acoustic system

A numerical model of a rectangular box cavity with a flexible plate with piezoelectric patches that is coupled to the acoustic domain of the cavity is developed using finite element (FE) method. Electromechanical interaction between the piezoelectric patches and the plate of the cavity is modeled through a coupled piezoelectric-structural model.

The finite element formulation of piezoelectric patches glued to the plate is dealt by laminated plate theory (Lim *et al.* 1999, Piefort 2001, Preumount 2002, and Abreu *et al.* 2004). The finite element formulation of the coupled structural and acoustic system has been studied extensively and is available in literature (Filippi 1983, Fahy and Gardonio 1987, Ohayon and Soize 2014). The coupled piezo-structural equations and coupled structural-acoustic equations can be combined to obtain coupled piezo-structural-acoustic model (Larbi *et al.* 2010, 2011). The structural and the acoustic domains of the cavity may have a strong or a weak coupling. However, for the cavities encountered in aerospace and automotive applications the coupling is rather weak and hence a one way structural-acoustic coupling is assumed in this paper. A typical flexible plate with two collocated piezoelectric patches, used as a sensor and actuator pair, glued to it is shown in Fig. 1.

The combined finite element equation that couples the piezoelectric, structural and acoustic domains can be written as

$$\begin{bmatrix} \mathbf{M}_T & \mathbf{0} & \mathbf{0} & \mathbf{0} \\ \mathbf{0} & \mathbf{0} & \mathbf{0} & \mathbf{0} \\ \mathbf{0} & \mathbf{0} & \mathbf{0} & \mathbf{0} \\ -\mathbf{S}^T & \mathbf{0} & \mathbf{0} & \mathbf{M}_A \end{bmatrix} \begin{Bmatrix} \ddot{\mathbf{w}} \\ \ddot{\phi}_a \\ \ddot{\phi}_s \\ \ddot{\mathbf{p}} \end{Bmatrix} + \begin{bmatrix} \mathbf{C}_S & \mathbf{0} & \mathbf{0} & \mathbf{0} \\ \mathbf{0} & \mathbf{0} & \mathbf{0} & \mathbf{0} \\ \mathbf{0} & \mathbf{0} & \mathbf{0} & \mathbf{0} \\ \mathbf{0} & \mathbf{0} & \mathbf{0} & \mathbf{C}_A \end{bmatrix} \begin{Bmatrix} \dot{\mathbf{w}} \\ \dot{\phi}_a \\ \dot{\phi}_s \\ \dot{\mathbf{p}} \end{Bmatrix} + \begin{bmatrix} \mathbf{K}_T & \mathbf{K}^a_{w\phi} & \mathbf{K}^s_{w\phi} & \mathbf{0} \\ \mathbf{K}^{a\,T}_{w\phi} & \mathbf{K}^a_{\phi\phi} & \mathbf{0} & \mathbf{0} \\ \mathbf{K}^{s\,T}_{w\phi} & \mathbf{0} & \mathbf{K}^s_{\phi\phi} & \mathbf{0} \\ \mathbf{0} & \mathbf{0} & \mathbf{0} & \mathbf{K}_A \end{bmatrix} \begin{Bmatrix} \mathbf{w} \\ \phi_a \\ \phi_s \\ \mathbf{p} \end{Bmatrix} = \begin{Bmatrix} \mathbf{g} \\ -q_a \\ -q_s \\ \mathbf{0} \end{Bmatrix} \tag{1}$$

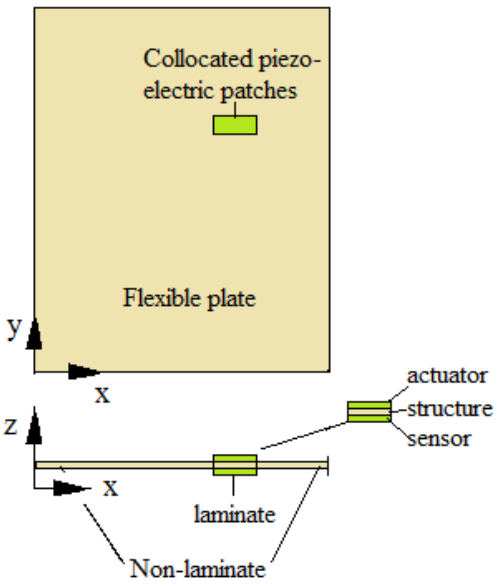

Fig. 1 Flexible plate with two collocated piezoelectric patches (piezo-structural system)

In the above equation **w** represents a vector of the structural degrees of freedom (which includes one transverse displacement and two rotations at each node of the structural FE mesh), ϕ_a and ϕ_s represent vectors of voltages on the piezoelectric patches used as the actuators and the sensors respectively and **p** represents a vector of the nodal acoustic pressures. Similarly, **g** represents a vector of the random disturbances acting on the cavity. q_a and q_s are vectors of the electric charges at the actuator and the sensor electrodes respectively. $\mathbf{M}_T$ and $\mathbf{K}_T$ are the combined structural and piezoelectric mass/inertia and stiffness matrices respectively, $\mathbf{M}_A$ and $\mathbf{K}_A$ are the acoustic mass/inertia and stiffness matrices respectively, **S** is the structure-acoustic coupling matrix, $\mathbf{C}_S$ and $\mathbf{C}_A$ are the structural and acoustic viscous damping matrices respectively, $\mathbf{K}^a_{w\phi}$ and $\mathbf{K}^s_{w\phi}$ are the electro-mechanical coupling matrices between the structure and the actuators and between the structure and the sensors respectively and $\mathbf{K}^a_{\phi\phi}$ and $\mathbf{K}^s_{\phi\phi}$ are the electric capacitance matrices of the actuators and the sensors respectively.

The various sub-matrices appearing in Eq. (1) are explained below. The flexible plate with piezoelectric patches consists of two distinct portions. One is laminated which consist of layers of piezoelectric material and the plate. The other is non-laminated portion which consist of only the flexible plate. The structural matrices for the laminated portion are developed using laminated plate theory taking into account piezoelectric constitutive relations. The structural matrices for the non-laminated portion are developed using Kirchhoff's thin plate bending theory (Petyt 2003 and Abreu *et al.* 2004). The structural matrices for the combined piezo-structural system are obtained by assembling the structural matrices for the laminated and the non-laminated portions of the system. Therefore, the mass matrix of the combined piezo-structural domain ($\mathbf{M}_T$),laminated portion ($\mathbf{M}_L$),the piezoelectric actuator ($\mathbf{M}_{act}$),the flexible plate ($\mathbf{M}_{str}$),the piezoelectric sensor ($\mathbf{M}_{sen}$) and of the non-laminated portion ($\mathbf{M}_{N\text{-}L}$) is written as,

$$\mathbf{M}_T = \mathbf{M}_L + \mathbf{M}_{N\text{-}L} \tag{2}$$

$$\mathbf{M}_L = \mathbf{M}_{act} + \mathbf{M}_{str} + \mathbf{M}_{sen} \tag{3}$$

$$\mathbf{M}_{act} = \sum \int \rho_{act} \mathbf{N}^T_{act} \mathbf{N}_{act} dV \tag{4}$$

$$\mathbf{M}_{str} = \sum \int \rho_{str} \mathbf{N}^T_{str} \mathbf{N}_{str} dV \tag{5}$$

$$\mathbf{M}_{sen} = \sum \int \rho_{sen} \mathbf{N}^T_{sen} \mathbf{N}_{sen} dV \tag{6}$$

$$\mathbf{M}_{N\text{-}L} = \sum \int \rho_{N-L} \mathbf{N}^T_{N-L} \mathbf{N}_{N-L} dV \tag{7}$$

Where ρ_{act}, ρ_{str} and ρ_{sen} are the densities of the actuator, structure and piezoelectric sensor respectively. ρ_{N-L} represents the density of the non-laminated portion of the piezo-structural system. $\mathbf{N}_{act}$, $\mathbf{N}_{str}$, $\mathbf{N}_{sen}$ and $\mathbf{N}_{N-L}$ are the shape function matrices for the piezoelectric actuator, structure, sensor and non-laminated portion of the piezo-structural system respectively.

Similarly, the stiffness matrix of the combined piezo-structural domain ($\mathbf{K}_T$), laminated portion ($\mathbf{K}_L$), the piezoelectric actuator ($\mathbf{K}_{act}$), the flexible plate ($\mathbf{K}_{str}$), the piezoelectric sensor ($\mathbf{K}_{sen}$) and of the non-laminated portion ($\mathbf{K}_{N\text{-}L}$) is written as

$$\mathbf{K}_T = \mathbf{K}_L + \mathbf{K}_{N\text{-}L} \tag{8}$$

$$\mathbf{K}_L = \mathbf{K}_{act} + \mathbf{K}_{str} + \mathbf{K}_{sen} \tag{9}$$

$$\mathbf{K}_{act} = \sum \int z^2 \mathbf{B}^T_{act} \mathbf{C}^E_{act} \mathbf{B}_{act} dV \tag{10}$$

$$\mathbf{K}_{str} = \sum \int z^2 \mathbf{B}^T_{str} \mathbf{C}^E_{str} \mathbf{B}_{str} dV \tag{11}$$

$$\mathbf{K}_{sen} = \sum \int z^2 \mathbf{B}^T_{sen} \mathbf{C}^E_{sen} \mathbf{B}_{sen} dV \tag{12}$$

$$\mathbf{K}_{N\text{-}L} = \sum \int z^2 \mathbf{B}^T_{N-L} \mathbf{C}^E_{N-L} \mathbf{B}_{N-L} dV \tag{13}$$

Where **B** and $\mathbf{C}^E$ are the strain-displacement and the material property matrices respectively.

The electro-mechanical coupling matrix between the plate and the piezoelectric actuator and sensor is written as

$$\mathbf{K}^a_{w\phi} = \sum \int -z \mathbf{B}^T_{str} \mathbf{e}^T_{act} \mathbf{B}_{\phi_{act}} dV \tag{14}$$

$$\mathbf{K}^s_{w\phi} = \sum \int -z \mathbf{B}^T_{str} \mathbf{e}^T_{sen} \mathbf{B}_{\phi_{sen}} dV \tag{15}$$

The electric capacitance matrix for the piezoelectric actuator and sensor is written as

$$\mathbf{K}^a_{\phi\phi} = \sum \int -z \mathbf{B}^T_{\phi_{act}} \zeta^S_{act} \mathbf{B}_{\phi_{act}} dV \tag{16}$$

$$\mathbf{K}^s_{\phi\phi} = \sum \int -z \mathbf{B}^T_{\phi_{sen}} \zeta^S_{sen} \mathbf{B}_{\phi_{sen}} dV \tag{17}$$

Where $\mathbf{e}_{act}$, $\mathbf{e}_{sen}$, ζ^S_{act}, ζ^S_{sen} are the piezoelectric strain coefficient and dielectric matrices at constant strain for actuator and sensor respectively. The $\sum$ sign in the above equations represents assembly over the finite elements of the laminated and non-laminated portions of the piezo-structural system.

The acoustic mass, stiffness and structural-acoustic coupling matrices (Filippi 1983) are written as follows

$$\mathbf{M}_{\mathrm{A}} = \sum \int \frac{1}{c^2} \mathbf{N}_{\mathrm{A}}^{\mathrm{T}} \mathbf{N}_{\mathrm{A}} \, dV \tag{18}$$

$$\mathbf{K}_{\mathrm{A}} = \sum \int \nabla \mathbf{N}_{\mathrm{A}}^{\mathrm{T}} \nabla \mathbf{N}_{\mathrm{A}} \, dV \tag{19}$$

$$\mathbf{S} = \sum \int \mathbf{N}_{\mathrm{S}}^{\mathrm{T}} \mathbf{N}_{\mathrm{A}} \, dA \tag{20}$$

Here $\mathbf{M}_{\mathrm{A}}$, $\mathbf{K}_{\mathrm{A}}$ and $\mathbf{S}$ are the mass, stiffness and structural-acoustic coupling matrices respectively. The summation signs in Eqs. (18) and (19) represent the assembly over the acoustic finite elements of the model, while the summation sign in Eq. (20) represents the assembly over those acoustic finite elements that have a face common with piezo-structural part. Here $\mathbf{N}_{\mathrm{A}}$ is the shape function matrix for the acoustic finite element. $\mathbf{N}_{\mathrm{S}}$ is the combined piezo-structural shape function matrix.

The structural and acoustic viscous damping matrices are computed from the corresponding modal data as follows

$$\mathbf{C}_{\mathrm{S}} = \boldsymbol{\psi}_S^{-T} \left[2\xi_{Si} \lambda_{Si} \right] \boldsymbol{\psi}_S^{-1} \tag{21}$$

$$\mathbf{C}_{\mathrm{A}} = \boldsymbol{\psi}_A^{-T} \left[2\xi_{Ai} \lambda_{Ai} \right] \boldsymbol{\psi}_A^{-1} \tag{22}$$

Where $\mathbf{C}_{\mathrm{S}}$ and $\mathbf{C}_{\mathrm{A}}$ are the structural and acoustic viscous damping matrices respectively. $\boldsymbol{\psi}_S$ and $\boldsymbol{\psi}_A$ are the mass normalized mode shape matrices of the structural and acoustic domains respectively. ξ_S and ξ_A are the damping coefficients of the structural and acoustic domains respectively while λ_S and λ_A are the eigenvalues of the structural and acoustic domains respectively.

3. State space model of the structural domain of the cavity

The combination of the structural model with the piezoelectric model is referred here as the plant model.

Following equations can be extracted from Eq. (1).

$$\mathbf{M}_{\mathrm{T}} \ddot{\mathbf{w}} + \mathbf{C}_{\mathrm{S}} \dot{\mathbf{w}} + \mathbf{K}_{\mathrm{T}} \mathbf{w} + \mathbf{K}_{\mathrm{w}\phi}^{\mathrm{a}} \phi_{\mathrm{a}} + \mathbf{K}_{\mathrm{w}\phi}^{\mathrm{s}} \phi_{\mathrm{s}} = \mathbf{g} \tag{23}$$

$$\mathbf{K}_{\mathrm{w}\phi}^{\mathrm{a}\ \mathrm{T}} \mathbf{w} + \mathbf{K}_{\phi\phi}^{\mathrm{a}} \phi_{\mathrm{a}} = -q_{\mathrm{a}} \tag{24}$$

$$\mathbf{K}_{\mathrm{w}\phi}^{\mathrm{s}\ \mathrm{T}} \mathbf{w} + \mathbf{K}_{\phi\phi}^{\mathrm{s}} \phi_{\mathrm{s}} = -q_{\mathrm{s}} \tag{25}$$

3.1 State space model of the plant in physical domain

After imposing the short circuit electric boundary conditions ($\phi_{\mathrm{s}} = 0$ but $q_{\mathrm{s}} \neq 0$) on the piezoelectric patches, Eq. (23) can be written as

$$\mathbf{M}_T \ddot{\mathbf{w}} + \mathbf{C}_S \dot{\mathbf{w}} + \mathbf{K}_T \mathbf{w} + \mathbf{K}_{w\phi}^{a} \phi_a = \mathbf{g} \tag{26}$$

The charge generated on the sensor electrodes is calculated as

$$q_s = -\mathbf{K}_{w\phi}^{s\ T} \mathbf{w} \tag{27}$$

If a charge amplifier is used, the output voltage is proportional to the electric charge in the sensor electrode.

$$\phi_s = -\frac{q_s}{C} \tag{28}$$

The sensor output voltage from the charge amplifier can be written as

$$\phi_s = S_{ca} \mathbf{K}_{w\phi}^{s\ T} \mathbf{w} \tag{29}$$

Where C is the capacitance and S_{ca} is the gain of the charge amplifier in *mV/pC*.

Eq. (26) can also be written as

$$\mathbf{M}_T \ddot{\mathbf{w}} + \mathbf{C}_S \dot{\mathbf{w}} + \mathbf{K}_T \mathbf{w} = \mathbf{g} - \mathbf{K}_{w\phi}^{a} \phi_a \tag{30}$$

$$\mathbf{M}_T \ddot{\mathbf{w}} = \mathbf{g} - \mathbf{K}_{w\phi}^{a} \phi_a - \mathbf{C}_S \dot{\mathbf{w}} - \mathbf{K}_T \mathbf{w} \tag{31}$$

The structural acceleration is obtained as

$$\ddot{\mathbf{w}} = \mathbf{M}_T^{-1} \mathbf{g} - \mathbf{M}_T^{-1} \mathbf{K}_{w\phi}^{a} \phi_a - \mathbf{M}_T^{-1} \mathbf{C}_S \dot{\mathbf{w}} - \mathbf{M}_T^{-1} \mathbf{K}_T \mathbf{w} \tag{32}$$

Choosing structural physical displacement $\mathbf{w}$ and structural physical velocity $\dot{\mathbf{w}}$ as state variables $\mathbf{w}_1$ and $\mathbf{w}_2$ respectively

$$\mathbf{w}_1(t) = \mathbf{w}(t) \quad \text{and} \quad \mathbf{w}_2(t) = \dot{\mathbf{w}}(t) \tag{33}$$

$$\dot{\mathbf{w}}_1(t) = \dot{\mathbf{w}}(t) = \mathbf{w}_2(t) \tag{34}$$

$$\dot{\mathbf{w}}_2(t) = \ddot{\mathbf{w}}(t) \tag{35}$$

Using Eqs. (32) and (35)

$$\dot{\mathbf{w}}_2(t) = \ddot{\mathbf{w}} = \mathbf{M}_T^{-1} \mathbf{g} - \mathbf{M}_T^{-1} \mathbf{K}_{w\phi}^{a} \phi_a - \mathbf{M}_T^{-1} \mathbf{C}_S \dot{\mathbf{w}} - \mathbf{M}_T^{-1} \mathbf{K}_T \mathbf{w} \tag{36}$$

The state space model of the plant in physical domain is given by

$$\begin{Bmatrix} \dot{\mathbf{w}}_1(t) \\ \dot{\mathbf{w}}_2(t) \end{Bmatrix} = \begin{bmatrix} \mathbf{0} & \mathbf{I} \\ -\mathbf{M}_{\mathrm{T}}^{-1} \mathbf{K}_T & -\mathbf{M}_{\mathrm{T}}^{-1} \mathbf{C}_{\mathrm{S}} \end{bmatrix} \begin{Bmatrix} \mathbf{w}_1(t) \\ \mathbf{w}_2(t) \end{Bmatrix} + \begin{bmatrix} \mathbf{0} & \mathbf{0} \\ \mathbf{M}_{\mathrm{T}}^{-1} & -\mathbf{M}_{\mathrm{T}}^{-1} \mathbf{K}_{w\phi}^{a} \end{bmatrix} \begin{Bmatrix} \mathbf{g} \\ \phi_a \end{Bmatrix} \tag{37}$$

The output equation with displacement, velocity, acceleration, sensor output voltage and charge accumulated on piezoelectric electrodes as outputs can be written as

$$\begin{Bmatrix} \mathbf{w} \\ \dot{\mathbf{w}} \\ \ddot{\mathbf{w}} \\ \phi_s \\ q_s \end{Bmatrix} = \begin{bmatrix} \mathbf{1} & \mathbf{0} \\ \mathbf{0} & \mathbf{1} \\ -\mathbf{M}_{\mathrm{T}}^{-1} \mathbf{K}_T & -\mathbf{M}_{\mathrm{T}}^{-1} \mathbf{C}_{\mathrm{S}} \\ S_{ca} \mathbf{K}_{w\phi}^{s\ T} & \mathbf{0} \\ -\mathbf{K}_{w\phi}^{s\ T} & \mathbf{0} \end{bmatrix} \begin{Bmatrix} \mathbf{w}_1(t) \\ \mathbf{w}_2(t) \end{Bmatrix} + \begin{bmatrix} \mathbf{0} & \mathbf{0} \\ \mathbf{0} & \mathbf{0} \\ \mathbf{M}_{\mathrm{T}}^{-1} & -\mathbf{M}_{\mathrm{T}}^{-1} \mathbf{K}_{w\phi}^{a} \\ \mathbf{0} & \mathbf{0} \\ \mathbf{0} & \mathbf{0} \end{bmatrix} \begin{Bmatrix} \mathbf{g} \\ \phi_a \end{Bmatrix} \tag{38}$$

3.2 State space model of the plant in modal domain

The state space model of the plant in modal domain is developed in this section. Transformation to modal coordinates is done using the mass normalized in-*vacuo* eigenvectors $\boldsymbol{\psi}_{\mathrm{S}}$ of the structure-piezo system

$$\mathbf{w} = \boldsymbol{\psi}_{\mathrm{S}}\boldsymbol{\eta}_{\mathrm{S}};\quad \dot{\mathbf{w}} = \boldsymbol{\psi}_{S}\dot{\boldsymbol{\eta}}_{\mathrm{S}};\quad \ddot{\mathbf{w}} = \boldsymbol{\psi}_{S}\ddot{\boldsymbol{\eta}}_{\mathrm{S}} \tag{39}$$

Substituting Eq. (39) into (30), pre-multiplying by $\boldsymbol{\psi}_{\mathrm{S}}^{\mathrm{T}}$ and making use of the orthogonality properties $\boldsymbol{\psi}_S^T\mathbf{M}_T\boldsymbol{\psi}_S = \mathbf{I}$, $\boldsymbol{\psi}_S^T\mathbf{K}_T\boldsymbol{\psi}_S = \boldsymbol{\lambda}_S^2$ and $\boldsymbol{\psi}_S^T\mathbf{C}_S\boldsymbol{\psi}_S = \boldsymbol{\Lambda}_S = \left[2\xi_S\lambda_S\right]$, we get the equation of motion of the plant in modal domain as

$$\mathbf{I}\ddot{\boldsymbol{\eta}}_{\mathrm{S}} + \boldsymbol{\Lambda}_{\mathrm{S}}\dot{\boldsymbol{\eta}}_{\mathrm{S}} + \boldsymbol{\lambda}_{\mathrm{S}}^2\boldsymbol{\eta}_{\mathrm{S}} = \boldsymbol{\psi}_{\mathrm{S}}^{\mathrm{T}}\left(\mathbf{g} - \mathbf{K}_{\mathrm{w}\phi}^{\mathrm{a}}\boldsymbol{\phi}_{\mathrm{a}}\right) \tag{40}$$

Choosing the structural modal displacements $\boldsymbol{\eta}_{\mathrm{S}}$ and the modal velocities $\dot{\boldsymbol{\eta}}_{\mathrm{S}}$ as state variables and representing them by $\boldsymbol{\beta}_1$ and $\boldsymbol{\beta}_2$ respectively, we get following state equation in the modal coordinates

$$\begin{Bmatrix}\dot{\boldsymbol{\beta}}_1\\ \dot{\boldsymbol{\beta}}_2\end{Bmatrix} = \begin{bmatrix}\mathbf{0} & \mathbf{I}\\ -\boldsymbol{\lambda}_{\mathrm{S}}^2 & -\boldsymbol{\Lambda}_{\mathrm{S}}\end{bmatrix}\begin{Bmatrix}\boldsymbol{\beta}_1\\ \boldsymbol{\beta}_2\end{Bmatrix} + \begin{bmatrix}\mathbf{0} & \mathbf{0}\\ \boldsymbol{\psi}_{\mathrm{S}}^{\mathrm{T}} & -\boldsymbol{\psi}_{\mathrm{S}}^{\mathrm{T}}\mathbf{K}_{\mathrm{w}\phi}^{\mathrm{a}}\end{bmatrix}\begin{Bmatrix}\mathbf{g}\\ \phi_{\mathrm{a}}\end{Bmatrix} \tag{41}$$

Where $\boldsymbol{\lambda}_{\mathrm{S}}^2$ is the matrix of eigenvalues of the structure-piezo system and $\boldsymbol{\Lambda}_{\mathrm{S}}$ is a diagonal matrix such that $\Lambda_{\mathrm{S}ii} = 2\xi_{\mathrm{S}i}\lambda_{\mathrm{S}i}$, with $\xi_{\mathrm{S}i}$ representing the viscous modal damping factors of the structure.

The output equation with modal displacement, modal velocity, modal acceleration, displacement, velocity, acceleration, and sensor output voltage as outputs is given by

$$\begin{Bmatrix}\boldsymbol{\eta}_S\\ \dot{\boldsymbol{\eta}}_S\\ \ddot{\boldsymbol{\eta}}_S\\ \mathbf{w}\\ \dot{\mathbf{w}}\\ \ddot{\mathbf{w}}\\ \phi_s\end{Bmatrix} = \begin{bmatrix}\mathbf{1} & \mathbf{0}\\ \mathbf{0} & \mathbf{1}\\ -\boldsymbol{\lambda}_S^2 & -\boldsymbol{\Lambda}_S\\ \boldsymbol{\psi}_S & \mathbf{0}\\ \mathbf{0} & \boldsymbol{\psi}_S\\ -\boldsymbol{\psi}_S\boldsymbol{\lambda}_S^2 & -\boldsymbol{\psi}_S\boldsymbol{\Lambda}_S\\ S_{ca}\mathbf{K}_{w\phi}^{s\ T}\boldsymbol{\psi}_S & \mathbf{0}\end{bmatrix}\begin{Bmatrix}\boldsymbol{\beta}_1\\ \boldsymbol{\beta}_2\end{Bmatrix} + \begin{bmatrix}\mathbf{0} & \mathbf{0}\\ \mathbf{0} & \mathbf{0}\\ \boldsymbol{\psi}_S^T & \boldsymbol{\psi}_S^T\mathbf{K}_{w\phi}^a\\ \mathbf{0} & \mathbf{0}\\ \mathbf{0} & \mathbf{0}\\ \boldsymbol{\psi}_S\boldsymbol{\psi}_S^T & -\boldsymbol{\psi}_S\boldsymbol{\psi}_S^T\mathbf{K}_{w\phi}^a\\ \mathbf{0} & \mathbf{0}\end{bmatrix}\begin{Bmatrix}\mathbf{g}\\ \phi_a\end{Bmatrix} \tag{42}$$

4. State space model of the acoustic domain of the cavity

In this section, the state space model of the acoustic domain of the vibro-acoustic cavity is developed. From Eq. (1) we get the equation of the acoustic domain as,

$$\mathbf{M}_{\mathrm{A}}\ddot{\mathbf{p}} + \mathbf{C}_{\mathrm{A}}\dot{\mathbf{p}} + \mathbf{K}_{\mathrm{A}}\mathbf{p} = \mathbf{S}^{\mathrm{T}}\ddot{\mathbf{w}} \tag{43}$$

Introducing modal transformation, $\mathbf{p} = \boldsymbol{\psi}_{\mathrm{A}}\boldsymbol{\eta}_{\mathrm{A}}$, with $\boldsymbol{\psi}_{\mathrm{A}}$ representing the mass normalized rigid-wall acoustic modes and making use of the orthogonal properties ($\boldsymbol{\psi}_{\mathrm{A}}^{\mathrm{T}}\mathbf{M}_{\mathrm{A}}\boldsymbol{\psi}_A = \mathbf{I}$, $\boldsymbol{\psi}_{\mathrm{A}}^{\mathrm{T}}\mathbf{K}_{\mathrm{A}}\boldsymbol{\psi}_A = \boldsymbol{\lambda}_{\mathrm{A}}^2$, and $\boldsymbol{\psi}_{\mathrm{A}}^{\mathrm{T}}\mathbf{C}_{\mathrm{A}}\boldsymbol{\psi}_A = \boldsymbol{\Lambda}_{\mathrm{A}}$) after pre-multiplying by the transpose of $\boldsymbol{\psi}_{\mathrm{A}}$, Eq. (43) can be written in the modal coordinates as

$$\mathbf{I}\ddot{\boldsymbol{\eta}}_{\mathrm{A}} + \boldsymbol{\Lambda}_{\mathrm{A}}\dot{\boldsymbol{\eta}}_{\mathrm{A}} + \boldsymbol{\lambda}_{\mathrm{A}}^2\boldsymbol{\eta}_{\mathrm{A}} = \boldsymbol{\psi}_{\mathrm{A}}^{\mathrm{T}}\mathbf{S}^{\mathrm{T}}\ddot{\mathbf{w}} \tag{44}$$

where $\boldsymbol{\lambda}_{\mathrm{A}}^2$ is the matrix of the eigenvalues of the rigid-wall acoustic modes and $\boldsymbol{\Lambda}_{\mathrm{A}}$ is a diagonal matrix such that $\Lambda_{\mathrm{A}ii} = 2\xi_{\mathrm{A}i}\lambda_{\mathrm{A}i}$, with $\xi_{\mathrm{A}i}$ representing the viscous modal damping factors of the acoustic domain.

Choosing the acoustic modal pressure $\boldsymbol{\eta}_{\mathrm{A}}$ and its first derivative $\dot{\boldsymbol{\eta}}_{\mathrm{A}}$ as state variables represented by $\boldsymbol{\eta}_{\mathrm{A1}}$ and $\boldsymbol{\eta}_{\mathrm{A2}}$ respectively, we get state equation in the modal coordinates as

$$\begin{Bmatrix}\dot{\boldsymbol{\eta}}_{\mathrm{A1}}\\ \dot{\boldsymbol{\eta}}_{\mathrm{A2}}\end{Bmatrix} = \begin{bmatrix}\mathbf{0} & \mathbf{I}\\ -\boldsymbol{\lambda}_{\mathrm{A}}^2 & -\boldsymbol{\Lambda}_{\mathrm{A}}\end{bmatrix}\begin{Bmatrix}\boldsymbol{\eta}_{\mathrm{A1}}\\ \boldsymbol{\eta}_{\mathrm{A2}}\end{Bmatrix} + \begin{bmatrix}\mathbf{0}\\ \boldsymbol{\psi}_{\mathrm{A}}^{\mathrm{T}}\mathbf{S}^{\mathrm{T}}\end{bmatrix}\ddot{\mathbf{w}} \tag{45}$$

Output equation for computing nodal acoustic pressure inside the cavity is written as

$$\mathbf{p} = \begin{bmatrix}\boldsymbol{\psi}_{\mathrm{A}} & \mathbf{0}\end{bmatrix}\begin{Bmatrix}\boldsymbol{\eta}_{\mathrm{A1}}\\ \boldsymbol{\eta}_{\mathrm{A2}}\end{Bmatrix} \tag{46}$$

5. Feedback control strategies for active control of noise

In this section, three feedback control strategies, namely, active vibration control using direct output feedback (AVC-DOFB), active vibration control using an LQR controller (AVC-LQR) and active structural-acoustic control using an LQR controller (ASAC-LQR) are presented.

5.1 Active vibration control using direct output feedback (AVC-DOFB)

In this strategy the objective is to reduce the vibrations of the cavity structre with the hope of reducing the noise radiated into the cavity. Therefore, this is an indirect noise control strategy. In control using direct output feedback (DOFB), the output of the sensor, after suitable conditioning, is directly fed to a controller having certain constant gain. The output of the controller is then fed to the actuator.

5.1.1 Open and closed loop system model

The state space model of the plate-piezo system, through Eqs. (37) and (38) is given by

$$\begin{Bmatrix}\dot{\mathbf{w}}_1(t)\\ \dot{\mathbf{w}}_2(t)\end{Bmatrix} = \begin{bmatrix}\mathbf{0} & \mathbf{I}\\ -\mathbf{M}_{\mathrm{T}}^{-1}\mathbf{K}_T & -\mathbf{M}_{\mathrm{T}}^{-1}\mathbf{C}_{\mathrm{S}}\end{bmatrix}\begin{Bmatrix}\mathbf{w}_1(t)\\ \mathbf{w}_2(t)\end{Bmatrix} + \begin{bmatrix}\mathbf{0} & \mathbf{0}\\ \mathbf{M}_{\mathrm{T}}^{-1} & -\mathbf{M}_{\mathrm{T}}^{-1}\mathbf{K}_{w\phi}^a\end{bmatrix}\begin{Bmatrix}\mathbf{g}\\ \phi_a\end{Bmatrix} \tag{47}$$

$$\begin{Bmatrix} \mathbf{w} \\ \dot{\mathbf{w}} \\ \ddot{\mathbf{w}} \\ \phi_s \\ q_s \end{Bmatrix} = \begin{bmatrix} \mathbf{1} & \mathbf{0} \\ \mathbf{0} & \mathbf{1} \\ -\mathbf{M}_T^{-1}\mathbf{K}_T & -\mathbf{M}_T^{-1}\mathbf{C}_S \\ S_{ca}\mathbf{K}_{w\phi}^{s\ T} & \mathbf{0} \\ -\mathbf{K}_{w\phi}^{s\ T} & \mathbf{0} \end{bmatrix} \begin{Bmatrix} \mathbf{w}_1(t) \\ \mathbf{w}_2(t) \end{Bmatrix} + \begin{bmatrix} \mathbf{0} & \mathbf{0} \\ \mathbf{0} & \mathbf{0} \\ \mathbf{M}_T^{-1} & -\mathbf{M}_T^{-1}\mathbf{K}_{w\phi}^{a} \\ \mathbf{0} & \mathbf{0} \\ \mathbf{0} & \mathbf{0} \end{bmatrix} \begin{Bmatrix} \mathbf{g} \\ \phi_a \end{Bmatrix} \quad (48)$$

The direct output feedback control law is taken as

$$\phi_a = -\mathrm{G}_d\phi_s - \mathrm{G}_v\dot{\phi}_s \quad (49)$$

Where G_d and G_v are the feedback gains corresponding to the sensor output voltage and its derivative respectively.

The short circuit sensor output voltage from Eq. (29) is

$$\phi_s = S_{ca}\mathbf{K}_{w\phi}^{s\ T}\mathbf{w} \quad (50)$$

Taking time derivative of above equation

$$\dot{\phi}_s = S_{ca}\mathbf{K}_{w\phi}^{s\ T}\dot{\mathbf{w}} \quad (51)$$

Second term on the R.H.S of the Eq. (47) can be expanded to obtain

$$\begin{Bmatrix} \dot{\mathbf{w}}_1(t) \\ \dot{\mathbf{w}}_2(t) \end{Bmatrix} = \begin{bmatrix} \mathbf{0} & \mathbf{I} \\ -\mathbf{M}_T^{-1}\mathbf{K}_T & -\mathbf{M}_T^{-1}\mathbf{C}_S \end{bmatrix} \begin{Bmatrix} \mathbf{w}_1(t) \\ \mathbf{w}_2(t) \end{Bmatrix} + \begin{bmatrix} \mathbf{0} \\ \mathbf{M}_T^{-1} \end{bmatrix} \mathbf{g} + \begin{bmatrix} \mathbf{0} \\ -\mathbf{M}_T^{-1}\mathbf{K}_{w\phi}^{a} \end{bmatrix} \phi_a \quad (52)$$

By putting Eq. (49) into Eq. (52), the following equation is obtained

$$\begin{Bmatrix} \dot{\mathbf{w}}_1(t) \\ \dot{\mathbf{w}}_2(t) \end{Bmatrix} = \begin{bmatrix} \mathbf{0} & \mathbf{I} \\ -\mathbf{M}_T^{-1}\mathbf{K}_T & -\mathbf{M}_T^{-1}\mathbf{C}_S \end{bmatrix} \begin{Bmatrix} \mathbf{w}_1(t) \\ \mathbf{w}_2(t) \end{Bmatrix} + \begin{bmatrix} \mathbf{0} \\ \mathbf{M}_T^{-1} \end{bmatrix} \mathbf{g} + \begin{bmatrix} \mathbf{0} \\ -\mathbf{M}_T^{-1}\mathbf{K}_{w\phi}^{a} \end{bmatrix} \left\{ -G_d\phi_s - G_v\dot{\phi}_s \right\} \quad (53)$$

The above equation can be further written as

$$\begin{Bmatrix} \dot{\mathbf{w}}_1(t) \\ \dot{\mathbf{w}}_2(t) \end{Bmatrix} = \begin{bmatrix} \mathbf{0} & \mathbf{I} \\ -\mathbf{M}_T^{-1}\mathbf{K}_T & -\mathbf{M}_T^{-1}\mathbf{C}_S \end{bmatrix} \begin{Bmatrix} \mathbf{w}_1(t) \\ \mathbf{w}_2(t) \end{Bmatrix} + \begin{bmatrix} \mathbf{0} \\ \mathbf{M}_T^{-1} \end{bmatrix} \mathbf{g} + \begin{bmatrix} \mathbf{0} \\ \mathbf{M}_T^{-1}\mathbf{K}_{w\phi}^{a} G_d\phi_s + \mathbf{M}_T^{-1}\mathbf{K}_{w\phi}^{a} G_v\dot{\phi}_s \end{bmatrix} \quad (54)$$

By substituting Eqs. (50) and (51) into above equation, we get

$$\begin{Bmatrix} \dot{\mathbf{w}}_1(t) \\ \dot{\mathbf{w}}_2(t) \end{Bmatrix} = \begin{bmatrix} \mathbf{0} & \mathbf{I} \\ -\mathbf{M}_T^{-1}\left(\mathbf{K}_T - \mathbf{K}_{w\phi}^{a} G_d S_{ca}\mathbf{K}_{w\phi}^{s\ T}\right) & -\mathbf{M}_T^{-1}\left(\mathbf{C}_S - \mathbf{K}_{w\phi}^{a} G_v S_{ca}\mathbf{K}_{w\phi}^{s\ T}\right) \end{bmatrix} \begin{Bmatrix} \mathbf{w}_1(t) \\ \mathbf{w}_2(t) \end{Bmatrix} + \begin{bmatrix} \mathbf{0} \\ \mathbf{M}_T^{-1} \end{bmatrix} \mathbf{g} \quad (55)$$

Eq. (55) can be written in compact form as

$$\begin{Bmatrix} \dot{\mathbf{w}}_1(t) \\ \dot{\mathbf{w}}_2(t) \end{Bmatrix} = \begin{bmatrix} \mathbf{0} & \mathbf{I} \\ -\mathbf{M}_T^{-1}\mathbf{K}_{new} & -\mathbf{M}_T^{-1}\mathbf{C}_{new} \end{bmatrix} \begin{Bmatrix} \mathbf{w}_1(t) \\ \mathbf{w}_2(t) \end{Bmatrix} + \begin{bmatrix} \mathbf{0} \\ \mathbf{M}_T^{-1} \end{bmatrix} \mathbf{g} \quad (56)$$

Where $\mathbf{K}_{new} = \mathbf{K}_T - \mathbf{K}_{w\phi}^{a} G_d S_{ca}\mathbf{K}_{w\phi}^{s\ T}$ and $\mathbf{C}_{new} = \mathbf{C}_S - \mathbf{K}_{w\phi}^{a} G_v S_{ca}\mathbf{K}_{w\phi}^{s\ T}$ are the stiffness and damping matrices of the plate-piezo system with control. After substituting Eq. (49) into Eq. (48), the output equation for the closed loop system is obtained as

$$\begin{Bmatrix} \phi_a \\ \ddot{\mathbf{w}} \end{Bmatrix} = \begin{bmatrix} -G_d S_{ca}\mathbf{K}_{w\phi}^{s\ T} & -G_v S_{ca}\mathbf{K}_{w\phi}^{s\ T} \\ -\mathbf{M}_T^{-1}\mathbf{K}_{new} & -\mathbf{M}_T^{-1}\mathbf{C}_{new} \end{bmatrix} \begin{Bmatrix} \mathbf{w}_1(t) \\ \mathbf{w}_2(t) \end{Bmatrix} + \begin{bmatrix} \mathbf{0} \\ \mathbf{M}_T^{-1} \end{bmatrix} \mathbf{g} \quad (57)$$

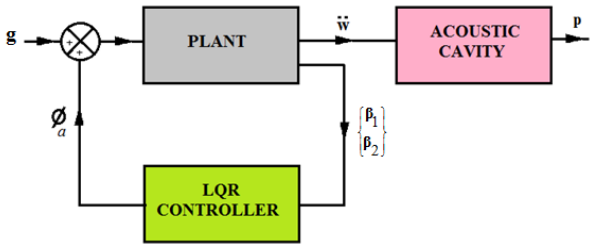

Fig. 2 AVC system using an LQR control strategy

5.2 Active vibration control using an LQR controller (AVC-LQR)

In this section an optimal control strategy in the form of a linear quadratic regulator (LQR) is used for active vibration control as shown through a block diagram in Fig. 2. The modal outputs (the modal displacements and the modal velocities) of the structure are fed to the LQR controller. It is assumed that all the modal states are available for feedback.

The state space equation in modal coordinates for the flexible plate with piezos (Eq. (41)) is given by

$$\begin{Bmatrix} \dot{\boldsymbol{\beta}}_1 \\ \dot{\boldsymbol{\beta}}_2 \end{Bmatrix} = \begin{bmatrix} \mathbf{0} & \mathbf{I} \\ -\boldsymbol{\lambda}_S^2 & -\boldsymbol{\Lambda}_S \end{bmatrix} \begin{Bmatrix} \boldsymbol{\beta}_1 \\ \boldsymbol{\beta}_2 \end{Bmatrix} + \begin{bmatrix} \mathbf{0} & \mathbf{0} \\ \boldsymbol{\psi}_S^{\mathrm{T}} & -\boldsymbol{\psi}_S^{\mathrm{T}}\mathbf{K}_{w\phi}^{\mathrm{a}} \end{bmatrix} \begin{Bmatrix} \mathbf{g} \\ \phi_a \end{Bmatrix} \quad (58)$$

Second term on the R.H.S of the above equation can be expanded to obtain,

$$\begin{Bmatrix} \dot{\boldsymbol{\beta}}_1 \\ \dot{\boldsymbol{\beta}}_2 \end{Bmatrix} = \begin{bmatrix} \mathbf{0} & \mathbf{I} \\ -\boldsymbol{\lambda}_S^2 & -\boldsymbol{\Lambda}_S \end{bmatrix} \begin{Bmatrix} \boldsymbol{\beta}_1 \\ \boldsymbol{\beta}_2 \end{Bmatrix} + \begin{bmatrix} \mathbf{0} \\ \boldsymbol{\psi}_S^{T} \end{bmatrix} \mathbf{g} + \begin{bmatrix} \mathbf{0} \\ -\boldsymbol{\psi}_S^{T}\mathbf{K}_{w\phi}^{a} \end{bmatrix} \phi_a \quad (59)$$

Eq. (59) can be written in compact form as

$$\dot{\boldsymbol{\beta}} = \mathbf{A}\boldsymbol{\beta} + \mathbf{B}_d\mathbf{g} + \mathbf{B}_c\phi_a \quad (60)$$

Where $\mathbf{A}$, $\mathbf{B}_d$, $\mathbf{B}_c$ are the state space matrices of the plant. $\boldsymbol{\beta} = \{\boldsymbol{\beta}_1 \quad \boldsymbol{\beta}_2\}^{\mathrm{T}}$ is the state vector of the modal displacements and velocities.

The LQR controller is an optimal controller that is based on minimization of an objective function. The objective function or the performance index denoted by J is written as

$$J = \int_0^\infty \left(\boldsymbol{\beta}^{\mathrm{T}}\mathbf{Q}\boldsymbol{\beta} + \phi_a^{\mathrm{T}}\mathbf{R}\phi_a\right)dt \quad (61)$$

Where $\mathbf{Q}$ and $\mathbf{R}$ are the weighting matrices in the LQR objective function. The matrix $\mathbf{Q}$ is a diagonal matrix and represents weight on the state vector. The r^{th} diagonal element represents weight on the r^{th} state variable. Similarly, the matrix $\mathbf{R}$ represents weighting for the control effort. The objective function for the LQR controller consists of two terms. In the method used here, the first term is dependent on the modal displacements and the modal velocities and therefore it

quantifies structural vibrations. The second term is dependent on the voltage control signal and therefore quantifies the control effort.

The algebraic Riccati equation needs to be solved to obtain the full state feedback gain matrix $\mathbf{K}$. The algebraic Riccati equation is given by

$$\mathbf{A}^{\mathrm{T}}\mathbf{P} + \mathbf{P}\mathbf{A} - \mathbf{P}\mathbf{B}_{\mathrm{c}}\mathbf{R}^{-1}\mathbf{B}_{\mathrm{c}}^{\mathrm{T}}\mathbf{P} + \mathbf{Q} = 0 \tag{62}$$

Solution of the above equation gives matrix **P** which then gives $\mathbf{K} = \mathbf{R}^{-1}\mathbf{B}_c^T\mathbf{P}$. The control law for the LQR controller is given by

$$\phi_a = -\mathbf{K}\boldsymbol{\beta} \tag{63}$$

Substituting control signal ϕ_a from Eq. (63) into Eq. (60), the state equation for the closed loop system is obtained as

$$\dot{\boldsymbol{\beta}} = \mathbf{A}\boldsymbol{\beta} - \mathbf{B}_c\mathbf{K}\boldsymbol{\beta} + \mathbf{B}_d\mathbf{g} \tag{64}$$

Above equation can be written as

$$\dot{\boldsymbol{\beta}} = \mathbf{A}_{CL}\boldsymbol{\beta} + \mathbf{B}_d\mathbf{g} \quad \text{Where} \quad \mathbf{A}_{CL} = \mathbf{A} - \mathbf{B}_c\mathbf{K} \tag{65}$$

Where $\mathbf{A}_{CL}$ is the closed loop state matrix for the LQR controller.

The output equation for the closed loop system is given by

$$\begin{Bmatrix} \phi_a \\ \ddot{\mathbf{w}} \end{Bmatrix} = \left[\begin{matrix} -\mathbf{K} \\ \left(\begin{bmatrix} -\boldsymbol{\psi}_S\boldsymbol{\lambda}_S^2 & -\boldsymbol{\psi}_S\boldsymbol{\Lambda}_S \end{bmatrix} + \boldsymbol{\psi}_S\boldsymbol{\psi}_S^T\mathbf{K}_{w\phi}^a\mathbf{K} \right) \end{matrix} \right] \boldsymbol{\beta} + \begin{bmatrix} \mathbf{0} \\ \boldsymbol{\psi}_S\boldsymbol{\psi}_S^T \end{bmatrix} \mathbf{g} \tag{66}$$

5.3 Active structural-acoustic control using an LQR controller (ASAC-LQR)

In this section, an LQR controller is designed by exploiting the knowledge of the structural-acoustic coupling of various structural and acoustic modes. This strategy is named as an active structural-acoustic control strategy because in this strategy, as explained below, the information about the coupling between the structural and the acoustic modes is utilized in the design of the LQR controller. This is distinct from the active vibration control strategies described in previous sections where no information about the acoustic domain is used in designing the controllers.

In this method, the weighting matrix **Q** in the LQR objective function is chosen based on the coupling coefficients between the structural and the acoustic modes of the cavity. The strategy aims to provide a higher relative weighting to those modes of the structure that have a higher level of coupling with the acoustic modes. The weighting matrix is computed as follows.

The structural-acoustic coupling matrix in the modal domain is given by

$$\bar{\mathbf{C}}_{AS} = \boldsymbol{\psi}_{\mathrm{A}}^{\mathrm{T}}\mathbf{S}^{\mathrm{T}}\boldsymbol{\psi}_{\mathrm{S}} \tag{67}$$

Where $\boldsymbol{\psi}_{\mathrm{A}}$ and $\boldsymbol{\psi}_{\mathrm{S}}$ are the matrices of the eigenvectors of the rigid-wall acoustic modes and in-*vacuo* structural modes and $\mathbf{S}$ is the structural-acoustic coupling matrix in the physical domain.

Let $\bar{\mathbf{C}}_{\mathrm{ij}}$ is the coupling between the i^{th} acoustic and the j^{th} structural mode. Weight $\mathbf{Q}_{rr}$ for the r^{th} structural mode is chosen by summing the values of its coupling coefficients with respect to all the acoustic modes in the frequency range of interest and then normalizing the sum. This is done using following equations.

$$\mathbf{Q}_{rr} = \frac{\bar{\mathbf{Q}}_{rr}}{\sum_{i=1}^{ns}\bar{\mathbf{Q}}_{ii}} \tag{68}$$

$$\bar{\mathbf{Q}}_{rr} = \sum_{i=1}^{na}\mathbf{C}_{i\,r} \tag{69}$$

The weights can be computed for $r = 1, 2, \ldots\ldots, ns$, where *ns* represents the number of structural modes in the frequency range of interest. The weights for various structural modes can be applied to both the modal displacements and the modal velocities or to only the modal velocities with zero weights to the modal displacements. Once the weighting matrix **Q** is defined as per the above strategy, the gain matrix **K** for the LQR controller can be obtained as explained in the previous section.

6. Numerical study

This section presents a numerical study of a 3-D rectangular box cavity with a flexible plate.

6.1 Details of the case study

A 3-D rectangular box cavity of size 0.261 m× 0.300 m×0.686 m backed by a flexible steel plate of size 0.261m×0.300m and thickness 0.001 m is considered. Fig. 3 shows the FE mesh of the piezo-structural-acoustic domain of the 3-D rectangular box vibro-acoustic cavity. The other five surfaces of the cavity are made of thick acrylic sheets and therefore are assumed to be rigid. The density, Young's modulus and Poisson's ratio for the plate material are taken as 7800 Kg m^{-3}, 2×10^{11} N m^{-2} and 0.3 respectively. The flexible plate is discretized using a mesh of 10×12 four-nodded Kirchhoff's thin plate bending finite elements that have three degrees of freedom at each of their nodes. This includes one out of plane displacement and two rotations. A modal damping factor of 0.005 is taken for all the modes of the plate with piezos.

A single pair of the collocated piezoelectric patches is considered in the study. The details of the piezoelectric patches are as follows. All the patches are P-876 A12 DuraAct piezoelectric patches. The dimensions are 0.0522×0.050 m^2 along *x* and *y* axes and the patches are 5×10^{-4} m thick. The Young's modulus, density, and Poisson's ratio are 23.3 GPa, 7800 Kg m^{-3} and 0.34 respectively. The piezoelectric strain coefficients e_{31} and e_{32} are equal to -8.9678 C m^{-2}. The dielectric constant ε_{33} is 6.6075×10^{-9} F m^{-1}. The piezoelectric patches on the flexible plate are modeled with classical lamination theory using piezo-electric constitutive relations and discretized into 2×2 four nodded rectangular bending elements with each

element having 12 mechanical DOFs and 2 electric DOFs (voltages). The details of coordinates of the corners of the rectangular piezoelectric patches in meters are as follows. Single piezoelectric patch: x_1,y_1=0.1566, 0.15, x_2,y_2=0.2088, 0.15, x_3,y_3=0.1566, 0.20, x_4, y_4=0.2088, 0.20.

The acoustic cavity is discretized using 10×12×14 eight-nodded solid hexahedral acoustic elements with acoustic pressure as a nodal degree of freedom. The total number of nodes is 2145. The density of the medium and the speed of sound are taken as 1.21 kg m^{-3} and 340 m s^{-1} respectively. A modal damping factor of 0.05 is taken for all the acoustic modes of the cavity.

An impulse force of 10N magnitude is applied at the node 103 (x = 0.0783 m and y = 0.225 m) on the flexible plate in this numerical study. Acoustic nodal pressure is predicted at node 1941 (having x-y-z coordinates 0.1044 m, 0.1750 m and 0.6370 m respectively) located at rear end of the cavity.

6.2 Design of controllers

6.2.1 Design of direct output feedback gain

This section presents a methodology to find the optimal value of the controller gain (G_v). The feedback gain G_d affects the stiffness of the system. For the study presented in this work it is assumed to be zero. Since the system under control is a flexible structure it has large number of poles. The method used here to chose the value of gain G_v is to see the effect of gain on the closed loop poles and choose a suitable value for it. Fig. 4 shows an overlay of pole map of the open and closed loop systems with G_v = 0.08. It is seen that the closed loop poles (shown with red color crosses) move to the left indicating increase in level of damping.

Table 1 shows the characteristics of the closed loop poles as gain G_v is varied over a certain range. The table shows the natural frequency, damping factor, settling time and peak overshoot of first eight poles. From this table it is seen that G_v = 0.08 gives a favorable damping, settling time and peak overshoot for most of the poles and hence this gain is chosen for the controller.

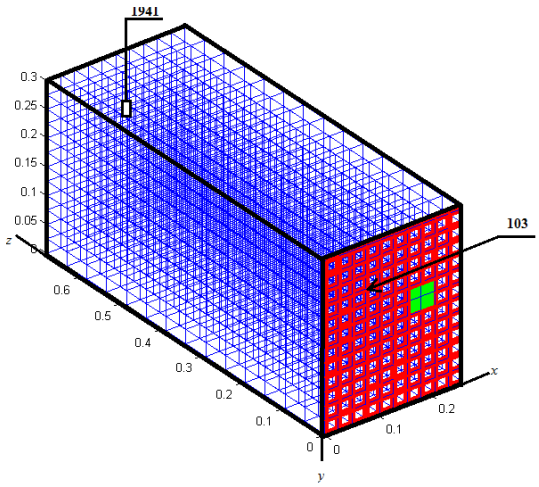

Fig. 3 FE mesh of piezo-structural-acoustic domain of the 3-D vibro-acoustic cavity

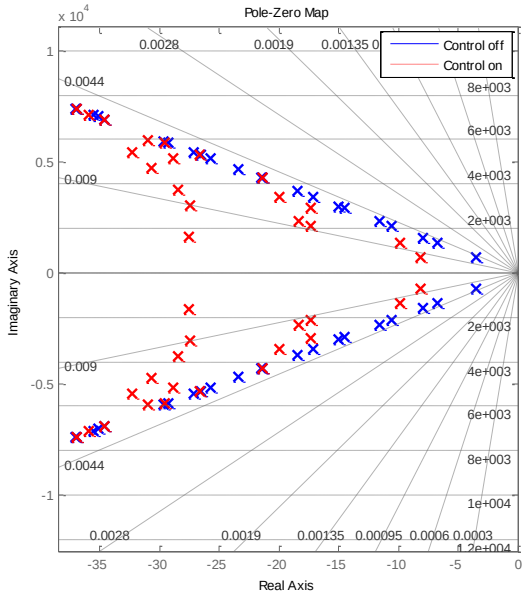

Fig. 4 Pole-zero plots at G_d = 0 and G_v = 0.08 (blue: open loop poles; red: closed loop poles)

*6.2.2 Calculation of **Q** matrix for AVC-LQR and for ASAC-LQR*

In AVC-LQR strategy, the weighting matrix **Q** is chosen to give equal weighting to the structural modes lying in the frequency range 0-545 Hz. A constant weight of 10000 is given to the modal displacements and the modal velocities of the first eighth structural modes. The weights for the remaining modes are taken zero. Eq. (70) shows the weighting matrix taken with the objective of controlling structural vibrations. This gives

$$\mathbf{Q} = \begin{bmatrix} \mathbf{q}_d & \mathbf{0} & \mathbf{0} & \mathbf{0} \\ \mathbf{0} & \mathbf{0} & \mathbf{0} & \mathbf{0} \\ \mathbf{0} & \mathbf{0} & \mathbf{q}_v & \mathbf{0} \\ \mathbf{0} & \mathbf{0} & \mathbf{0} & \mathbf{0} \end{bmatrix}, \quad \mathbf{R} = 0.0001 \tag{70}$$

$$\mathbf{q}_d = \mathrm{diag}\begin{bmatrix} 10000 & 10000 & 10000 & 10000 & 10000 & 10000 & 10000 & 10000 \end{bmatrix}_{8\times 8}$$

$$\mathbf{q}_v = \mathbf{q}_d$$

Modal structural-acoustic coupling coefficients $\bar{\mathbf{C}}_{ij}$ are first computed to frame the weighting matrix **Q** for the control strategy ASAC-LQR. Table 2 shows the modal coupling coefficients showing coupling between the i^{th} acoustic and the j^{th} structural mode. It is seen that the coefficients $\bar{\mathbf{C}}_{11}$, $\bar{\mathbf{C}}_{15}$, $\bar{\mathbf{C}}_{16}$, $\bar{\mathbf{C}}_{21}$, $\bar{\mathbf{C}}_{25}$, and $\bar{\mathbf{C}}_{26}$ are relatively large, which means that the structural modes **S1**, **S5** and **S6** are strongly coupled with the first and second acoustic modes (**A1** and **A2**) and therefore can radiate higher levels of noise. Eq. (71) shows the weighting matrix **Q** computed using the method described in section 5.3 and Table 2.

Table 1 Characteristics of various closed loop poles as a function of G_v

Pole No.	Natural Frequency (Hz)	Damping factor, settling time and peak overshoot	Feedback gain G_v							
			0	0.001	0.01	0.08	0.1	1.0	1e+3	1e+5
1	111.19	ξ	0.005	0.0052	0.006	0.011	0.011	0.005	0.0049	0.0049
		Ts (sec)	1.14	1.10	0.85	0.49	0.50	0.95	1.14	1.14
		PO (%)	98.4	98.4	97.9	96.4	96.5	98.2	98.5	98.5
2	213.24	ξ	0.005	0.0052	0.007	0.007	0.006	0.005	0.0049	0.0049
		Ts (sec)	0.59	0.57	0.44	0.40	0.42	0.57	0.59	0.59
		PO (%)	98.4	98.4	97.9	97.7	97.8	98.4	98.4	98.4
3	251.26	ξ	0.005	0.006	0.014	0.016	0.015	0.006	0.0048	0.0048
		Ts (sec)	0.50	0.42	0.18	0.14	0.16	0.41	0.50	0.50
		PO (%)	98.4	98.1	95.7	94.8	95.4	98.1	98.5	98.5
4	334.65	ξ	0.005	0.0054	0.009	0.008	0.007	0.005	0.0049	0.0049
		Ts (sec)	0.38	0.35	0.21	0.23	0.24	0.36	0.38	0.38
		PO (%)	98.4	98.3	97.3	97.5	97.6	98.4	98.5	98.5
5	369.45	ξ	0.005	0.0053	0.008	0.008	0.007	0.005	0.0049	0.0049
		Ts (sec)	0.34	0.32	0.21	0.21	0.23	0.32	0.34	0.34
		PO (%)	98.4	98.3	97.5	97.6	97.7	98.4	98.5	98.5
6	461.69	ξ	0.005	0.0054	0.008	0.006	0.006	0.005	0.0049	0.0049
		Ts (sec)	0.275	0.251	0.16	0.23	0.23	0.272	0.275	0.275
		PO (%)	98.4	98.3	97.4	98.2	98.2	98.4	98.5	98.5
7	477.34	ξ	0.005	0.0057	0.011	0.009	0.008	0.005	0.0048	0.0048
		Ts (sec)	0.26	0.23	0.11	0.14	0.16	0.25	0.272	0.272
		PO (%)	98.4	98.2	96.4	97.2	97.5	98.4	98.5	98.5
8	545.07	ξ	0.005	0.0052	0.007	0.006	0.005	0.005	0.0049	0.0049
		Ts (sec)	0.23	0.22	0.16	0.20	0.20	0.23	0.23	0.23
		PO (%)	98.4	98.4	97.8	98.2	98.3	98.5	98.5	98.5

Table 2 Modal structural-acoustic coupling coefficients ($\bar{\mathbf{C}}_{ij}$)

Structural Modes	Frequency of piezo-structural modes (Hz)	Modal structural- acoustic coupling coefficients	
		Acoustic modes	
		A1(250.5 Hz)	***A2(504.2 Hz)***
S1	111.19	**142.33**	**-144.13**
S2	213.23	7.09	-7.18
S3	251.25	10.43	-10.56
S4	334.64	2.14	-2.17
S5	369.45	**-64.31**	**65.12**
S6	461.69	**-63.15**	**63.95**
S7	477.34	-0.34	0.34
S8	545.07	-7.12	7.21

$$\mathbf{Q} = \begin{bmatrix} \mathbf{q}_d & \mathbf{0} & \mathbf{0} & \mathbf{0} \\ \mathbf{0} & \mathbf{0} & \mathbf{0} & \mathbf{0} \\ \mathbf{0} & \mathbf{0} & \mathbf{q}_v & \mathbf{0} \\ \mathbf{0} & \mathbf{0} & \mathbf{0} & \mathbf{0} \end{bmatrix} \tag{71}$$

$$\mathbf{q}_d = \mathrm{diag}\begin{bmatrix} 38300 & 1900 & 2800 & 500 & 17300 & 17000 & 92 & 1900 \end{bmatrix}_{8\times 8}$$

$$\mathbf{q}_v = \mathbf{q}_d$$

6.3 Closed loop performance by three feedback control strategies

In this section the closed loop performance using the three feedback control strategies is compared. Fig. 5 shows the output of the piezoelectric sensor with and without control. Fig. 6 shows the acoustic pressure at node 1941 (Fig. 3) inside the cavity with and without control. It is observed from these figures that the sensor ouput voltage as well as the acoustic pressure inside the cavity have reduced after control. This demonstrates that the active vibration control strategy using direct output feedback (AVC-DOFB) to indirectly achieve reduction in interior noise could be a useful strategy.

Fig. 7 shows a comparison of modal velocities of the first and seventh structural modes with and without control using AVC-LQR and ASAC-LQR control strategies. It is observed that using ASAC-LQR control strategy, the first structural mode, (which has high coupling coefficients) damps more quickly as compared to control using AVC-LQR strategy. Similarly, the seventh structural mode (which has low coupling coefficients) is allowed to damp slowly by ASAC-LQR control strategy. However, the AVC-LQR strategy tends to give equal importance to this structural mode.

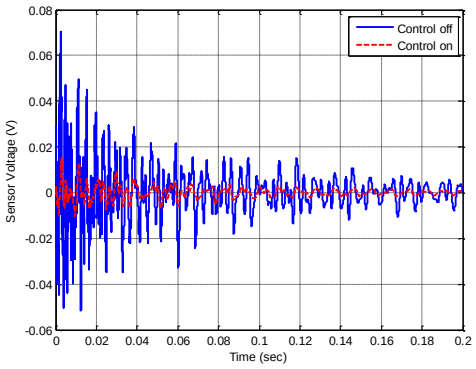

Fig. 5 Open and closed loop sensor output voltage (G_d =0 and G_v = 0.08)

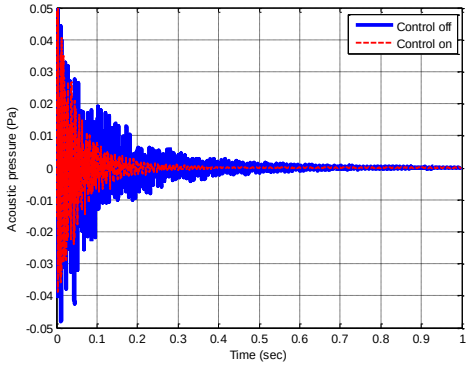

Fig. 6 Open and closed loop acoustic pressure at node number 1941 inside the cavity

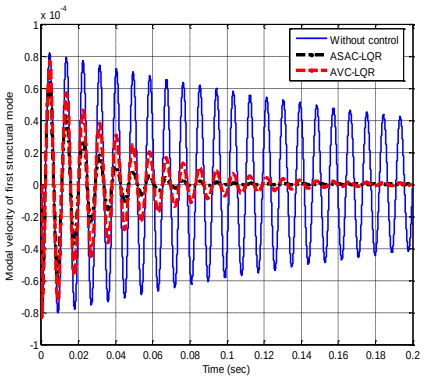

(a) First structural mode

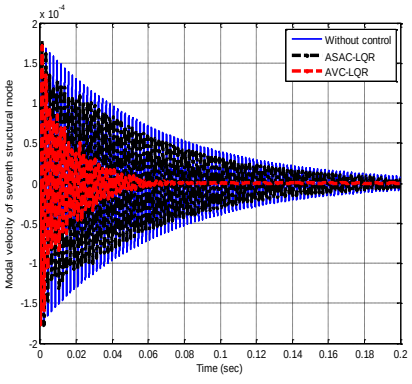

(b) Seventh structural mode

Fig. 7 Structural modal velocity

A comparison of freqeuncy response functions with and without control is further made using the three methods to study their performnace over the whole freqeuncy range of interest. The FRFs are computed with respect to a common sinusoidal force disturbance of unit amplitude acting on the plate. Figs. 8 and 9 show respectively FRFs of the nodal acceleration of the structure at node number 103 and nodal acoustic pressure at node number 1941 inside the vibro-acoustic cavity. In Fig. 8, the structural resonances of the system are identified with symbols **S1** to **S7**. The effect of the AVC-DOFB control strategy is seen to be distributed through the freqeuncy range. The AVC-LQR strategy tends to give equal importance to all the structural modes (Eq. (70)). The choice of weighting matrix **Q** has governed this kind of behavior of the controller. İt is observed that ASAC-LQR control strategy, damps modes **S1**, **S5** and **S6** more as compared to control using AVC-DOFB and AVC-LQR strategy. This is because the LQR controller based on the structural-acoustic coupling coefficients gives more importance to damp those structural modes that matter more for its cost function. The choice of weighting matrix **Q** as explained in previous section governed this behavior of the controller (Table 2 and Eq. (71)). A similiar behavior is seen in Fig. 9 the acosutic poressure due to the structural modes **S1**, **S5** and **S6** is significantly reduced.

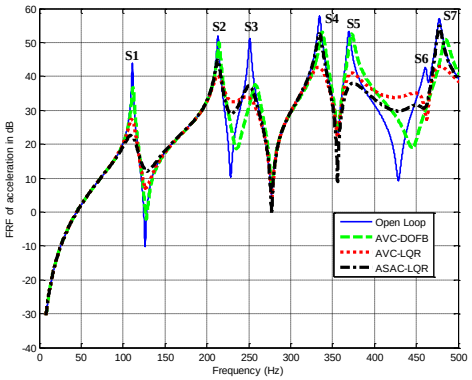

Fig. 8 Comparison of frequency response function of the acceleration of the structure in dB with and without control

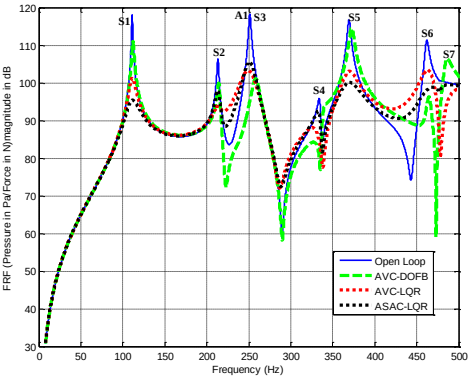

Fig. 9 Comparison of frequency response function (Pressure in Pa/ Force in N) of acoustic nodal pressure in dB with and without control

7. Conclusions

This paper presents comparison of three feedback control strategies for active noise control. The first two strategies i.e., control using direct output feedback and using an LQR controller are indirect strategies in which noise reduction is achieved through active vibration control. The third strategy is an active structural-acoustic control strategy. It is an LQR based optimal control strategy in which the information about the coupling between the various structural and the acoustic modes is used to design the controller.

Numerical studies on the 3-D rectangular box cavity are carried out and a comparison of structural vibration and acoustic pressure is carried out with and without the controllers. The control strategy based on direct output feedback is simple and easy to implement strategy but disregards the role of structural modes in generating the noise. The AVC-LQR control strategy tries to consume the control effort to damp all the structural modes. It is seen that the ASAC-LQR control strategy utilizes the control effort more intelligently by adding higher damping to those structural modes that matter more for reducing the interior noise.

Acknowledgments

The financial support for this work under the project DARO/08/1051606/M/I provided by Aeronautics Research and Development board (Structural panel), Ministry of Defense, Government of India, is gratefully acknowledged.

References

Abreu, G.L.C.M., Ribeiro, J.F. and Steefen, Jr. V. (2004), "Finite element modeling of a plate with localized piezoelectric sensors and actuators" , *J. Brazil Soc. of Mech. Sci. Eng*., **26**(2), 117-128.

Fahy, F. and Gardonio, P. (1987), Sound and structural vibration: Radiation, Transmission and Response, Academic press, London.

Filippi, P. (1983), Theoretical Acoustics and Numerical Techniques CISM Courses and Lectures, Springer-Verlag, Wien, New York, NY, USA.

Fuller, C.R. and Flotow, V. (1995), "Active control of sound and vibration", *IEEE Cont. Syst*., **15**(6), 9-19.

Larbi, W., Deu, J.F. and Ohayon, R. (2011), "Finite element formulation of smart piezoelectric composite plates coupled with acoustic fluid", *Comput. Struct*., **94**, 501-509.

Larbi, W., Deu, J.F., Ciminello, M. and Ohayon, R. (2010), "Structural-Acoustic Vibration reduction using switched shunt Piezoelectric patches: A finite element analysis", *J. Vib. Acoust*., **132**(5), 1-9.

Li, D.S. and Cheng, L. (2010), "The design of synthesized structural acoustic sensors for active control of interior noise with experimental validation", *J. Sound Vib*., **329**(2), 123-139.

Lim, Y.H., Gopinathan, S.V., Varadan, V.V. and Varadan, V.K. (1999), "Finite element simulation of smart structures using an optimal output feedback controller for vibration and noise control", *Smart Mater. Struct*., **8**(3), 324-337.

Morand, H. and Ohayon, R. (1995), Fluid-Structure Interaction, Wiley.

Ohayon, R. and Soize, C. (2014), Advanced Computational Vibro-acoustics, Cambridge University Press.

Petyt, M. (2003), Introduction to finite element vibration analysis, Cambridge university press.

Piefort, V. (2001), "Finite element modeling of piezoelectric active structures: some applications in vibro-acoustics".

Preumount, A. (2002), Vibration control of active structures, an introduction, Springer.

Ray, M.C., Faye, A., Patra, S. and Bhattacharyya, R. (2009), "Theoretical and experimental investigations on the active structural–acoustic control of a thin plate using a vertically reinforced 1-3 piezoelectric composite", *Smart Mater. Struct*., **18**, 1-13.

Song, C.K., Hwang, J.K., Lee, J.M. and Hedric, K.J. (2003), "Active vibration control for structural–acoustic coupling system of a 3-D vehicle cabin model", *J. Sound Vib*., **267**(4), 851-865.

Tanaka, N. and Kobayashi, K. (2006), "Cluster control of acoustic potential energy in a structural/acoustic cavity", *J. Acoust. Soc. Am*., **119**(5), 2758-2771.

CY